Prediction of Strong Solvatochromism in a Molecular Photocatalyst**

Miftahussurur Hamidi Putra,[a] Benedikt Bagemihl,[b] Sven Rau,[b] and Axel Groß*[c]

Based on quantum chemical calculations, we predict strong solvatochromism in a light-driven molecular photocatalyst for hydrogen generation, that is we show that the electronic and optical properties of the photocatalyst strongly depend on the solvent it is dissolved in. Our calculations in particular indicate a solvent-dependent relocation of the highest occupied molecular orbital (HOMO). Ground-state density functional theory and linear response time-dependent density functional theory calculations were applied in order to investigate the influence of implicit solvents on the structural, electronic and optical properties of a molecular photocatalyst. Only at high dielectric constants of the solvent, is the HOMO located at the metal center of the photosensitizer, whereas at low dielectric constants the HOMO is centered at the metal atom of the catalytically active complex. We elucidate the electronic origins of this strong solvatochromic effect and sketch the consequences of these insights for the use of photocatalysts in different environments.

Introduction

The efficient direct conversion of sunlight into valuable chemicals is challenging but has the potential to significantly contribute to a carbon-emission-free energy economy.[1] Recent years have witnessed an increased understanding of the mechanisms operative in photochemical molecular devices which combine a photosensitizer and a catalyst connected by an electron relay.[2–9] The operation of such molecular devices requires the presence of solvents, and as many molecular complexes are insoluble in aqueous media, often organic solvents are used.[4] Although it is known that the activity of photocatalysts is influenced by the properties of the solvent,[5] it is fair to say that a systematic understanding of this influence is

[a] M. H. Putra
Institute of Theoretical Chemistry, Ulm University
89069 Ulm (Germany)

[b] B. Bagemihl, Prof. Dr. S. Rau
Institute of Inorganic Chemistry I,
Materials and Catalysis, Ulm University
89069 Ulm (Germany)

[c] Prof. Dr. A. Groß
Institute of Theoretical Chemistry, Ulm University
89069 Ulm (Germany)
and
Helmholtz Institute Ulm (HIU),
Electrochemical Energy Storage
89069 Ulm (Germany)
E-mail: Axel.Gross@uni-ulm.de
Homepage: https://www.uni-ulm.de/theochem

[**] A previous version of this manuscript has been deposited on a preprint server (https://doi.org/10.26434/chemrxiv-2023-qv22c).

Supporting Information for this article is available on the WWW under https://doi.org/10.1002/chem.202302643

still lacking. Here we show that the polarity of a solvent represented by its dielectric constant can strongly affect the electronic and thus also the photocatalytic properties of photoactive molecular complexes.

In particular ruthenium-based complexes such as [(tbbpy)$_2$Ru(tpphz)PtI$_2$]$^{2+}$ (tbbpy = 4,4'-di-tert-butyl-2,2'-bipyridine, tpphz = tetrapyrido[3,2-a:2',3'-c:3''''-h:2''',3'''-j]phenazine) denoted by RuPtI$_2$ in the following, have successfully been used as the photosensitizer in photochemical molecular devices.[3,4,10] RuPtI$_2$ is one of the most active supramolecular photocatalysts for hydrogen evolution incorporating photosensitizer, bridging ligand and catalysts within one molecular structure. The recently established novel active repair mechanism for this catalyst leads to a boost in attainable catalytic activity with triethylamine (TEA) as electron donor and acetonitrile water mixtures as solvents.[11] The catalytic efficiency of the light-driven hydrogen evolution reaction of RuPtI$_2$ and the related RuPdCl$_2$ is strongly dependent on several factors such as the nature of the sacrificial electron donor[12] and supramolecular aggregation phenomena.[13–15] The interaction with polyaromatic supramolecular activators via π-π bonding with the bridging ligand led to a reduction in the induction phase and an improved initial turnover frequency (TOF) and turnover number (TON) for RuPdCl$_2$.[13] The nature of the applied solvent mixtures has a profound effect on the attainable catalytic activity.[16–18] Whereas in pure acetonitrile-TEA mixtures TONs of 56 are possible, increasing the water content leads to TONs of more than 200. However, it is not clear whether these effects stem from manipulation of the photophysics of the light-driven electron transfer due to solvatochromic effects[16] or from substrate limitations for the actual catalytic hydrogen evolution process.[17,18]

Here we concentrate on solvatochromic effects caused by the medium surrounding the photocatalytically active complexes which may modify its electronic and optical properties. Rutheniumpolypyridyl complexes have been shown to exhibit a negative solvatochromism, that is a blueshift of the UV-vis

Chemistry–A European Journal

Research Article
doi.org/10.1002/chem.202302643

Chemistry Europe
European Chemical
Societies Publishing

absorption bands in water compared to organic solvents[19] which has been reproduced in time-dependent density functional theory calculations and has been related to a decreased dipole moment in the excited state.[20] Such a blue shift has also been obtained in TD-DFT calculations of ruthenium(II) polypyridine-type complexes.[21] Solvent-induced shifts are typically assumed to be due to dipole-dipole interactions between polar molecules and a polarizable medium,[22] as found for a wide range of molecules.[22–26]

We will show that also photocatalytic molecular devices such as RuPtI$_2$ can exhibit a strong solvatochromism. In this molecule, [(tbbpy)$_2$Ru]$^{2+}$ acts as the photosensitizer (PS), (tpphz) is the bridging ligand (BL) and PtI$_2$ the catalytically active center (CAT), as illustrated in Figure 1. The expected photochemical mechanism in such photocatalysts is assumed to consist of the following steps: (i) A photon excites an electron in the Ru^{II} metal center which creates a metal-to-ligand charge-transfer (MLCT) state residing at the bridging ligand and bipyridine, (ii) ultrafast intersystem crossing (ISC) and excited state relaxation processes generate a population of triplet MLCT state(s) localized on the tpphz bridging ligand, and (iii) an electron transfer to the PtI$_2$ catalyst occurs and forms a charge-separated (CS) state.[27] As this photochemical molecular device consists of two metal centers, further complexity is added to the polarization mechanism responsible for solvatochromic effects. For example, electronic density can be shifted from the activated catalytic center to the bridging ligand upon visible-light irradiation thus reducing the catalytic activity.[28]

We will first present our quantum chemical calculations based on density functional theory (DFT) and time-dependent density functional theory (TDDFT) of the photocatalyst. The presence of the solvent has been taken into account using implicit solvent models. The findings of the quantum chemical calculations have been carefully analyzed in terms of the underlying electronic structure of the molecular complexes. Finally, we will discuss the implications of our findings for the operation of photocatalytic molecular devices.
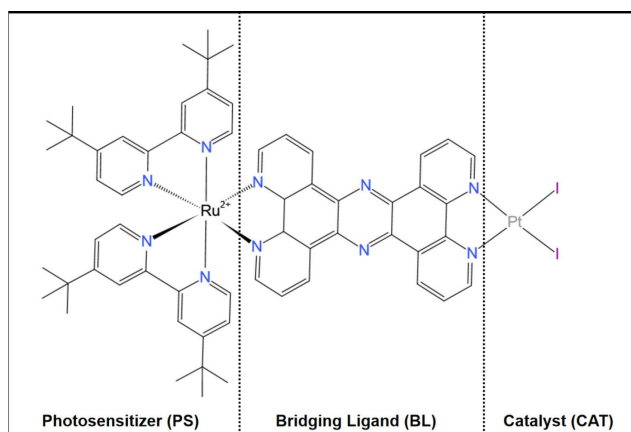
Results and Discussion

As a first step, we determined the structure of the RuPtI$_2$ monomer complex in the gas-phase and compared it with its optimized structure embedded in implicit solvents with dielectric constants up to $\varepsilon = 78.36$ corresponding to water. In detail, we have considered implicit solvents with dielectric constants corresponding to benzene, chlorobenzene, dichloroethane (DCE), acetone, ethanol (EtOH), methanol (MeOH), acetonitrile (MeCN), dimethylsulfoxide (DMSO), and water. In order to quantify the structural changes due to the presence of the solvent, we determined the change in the bond lengths ($|\Delta r_i|$):

$$|\Delta r_i| = \left| r_i^{\text{solvent}} - r_i^{\text{gas}} \right|, \tag{1}$$

and the bond angles ($|\gamma_i|$):

$$|\Delta \gamma_i| = \left| \gamma_i^{\text{solvent}} - \gamma_i^{\text{gas}} \right|, \tag{2}$$

with respect to the various bond lengths and angles of the complex.

In Figure 2, we plot both the maximum value and the mean value averaged over all bonds for the bond distances according to Equation (1) (panel a) and the bond angles according to Equation (2) (panel b) for all considered solutes. Overall we find rather small structural changes of the RuPtI$_2$ complex upon embedding it in the implicit solvent. On the average, the change in the bond distances is below 2.5×10^{-3} Å and the change in the bond angles is below 0.3°. Still, there are maximum changes of up to 0.05 Å in the bond distances and of up to 2° in the bond angles. Interestingly, these maximum changes are found in the Pt-I distance and the I-Pt-I bond angle of the catalytically active PtI$_2$ moiety. Obviously, the presence of the implicit solvent has the largest impact on the rather ionic bonds of the catalysts protruding into the solvent. However, overall we can conclude that the presence of the solvent has only a small influence on the geometric structure of the photoactive complex.

In contrast to the structural properties, the electronic properties depend sensitively on the dielectric constant of the electrolyte. In Figure 3a, the energy levels of the RuPtI$_2$ complex close to the HOMO–LUMO gap determined using the Gaussian 16 code[29] are plotted together with a color coding denoting the electron localization. First of all note that the HOMO levels are typically located at metal centers, whereas the LUMO levels belong to organic moieties. Very surprisingly, in the gas-phase and for weakly polar electrolytes, the HOMO is localized at the catalyst and not at the Ru atom. Hence, in the gas-phase low-energy excitations do not originate from the photosensitizer, as usually expected, but rather from the catalyst. Only starting with dichloroethane, that is at $\varepsilon \approx 10$, the HOMO becomes localized at the metal center of the photoactive Ru complex. In contrast, the LUMO is located at the phenazine part of the bridging ligand over the whole range of considered dielectric constants.

It is noteworthy that ruthenium complexes with oligopyridophenazine ligands show an optically accessible local LUMO
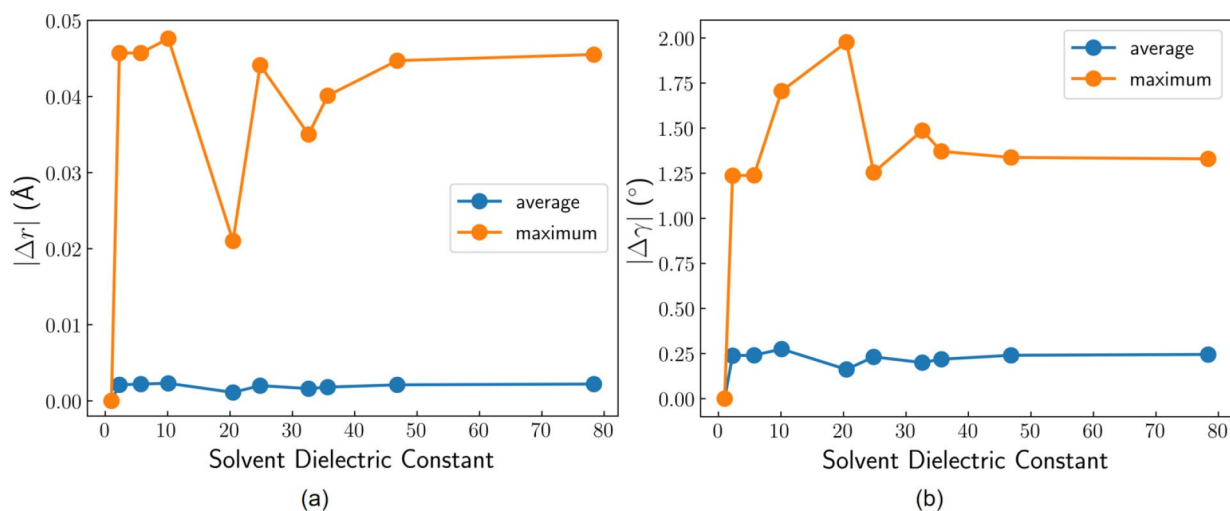

Figure 1. Illustration of the structure of the RuPtI$_2$ photocatalyst.

Figure 2. Maximum and average structural changes of the RuPtI$_2$ photocatalyst upon embedding it in various solvent compared to the optimum gas-phase structure with respect to the bond distances (a) and the bond angles (b).
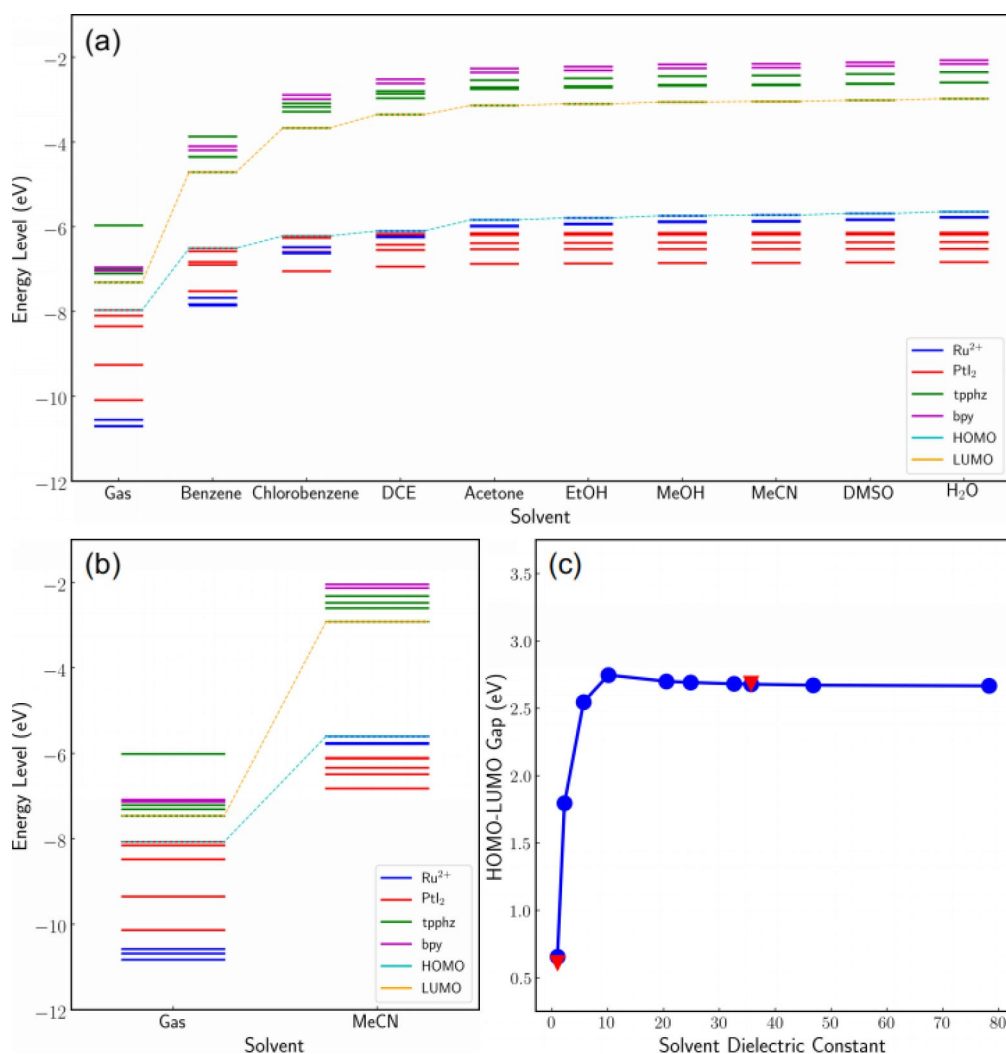

Figure 3. Calculated change in the electronic structure of the RuPtI$_2$ photocatalyst due to the presence of an implicit solvent. Occupied and unoccupied energy levels of the RuPtI$_2$ complex calculated using (a) the Gaussian 16 and (b) the FHI-AIMS code. The color coding indicates the projection of the one-particle states onto the Ru^{2+} metal center, the PtI$_2$ catalyst, the bridging ligand (tpphz) and bipyridine (bpy). The solvents are ordered according to their dielectric constant, and the corresponding HOMO and LUMO levels are connected by the yellow and light blue line, respectively. c) HOMO–LUMO gaps of RuPtI$_2$ as a function of the dielectric constant of the implicit solvent using both codes with the order of the solvents being the same as in panel a.

at the ruthenium coordinated bipyridine part of the ligand and a LUMO which is significantly lower in energy at the phenazine moiety. Direct optical population of the latter is not feasible.[30] Upon photoactivation of the ruthenium center, the excited electron becomes transferred to the bridging ligand. However, in contrast to the typically assumed picture of the photochemical mechanism in photocatalysts,[27] at low dielectric constants the initial metal-to-ligand charge transfer does not occur from the Ru^{II} metal center, but rather from the metal center of the catalyst. Figure 3a also reveals that all considered electronic levels move to higher energies with increasing dielectric constant. However, this dependence is least pronounced at the highest occupied state localized at the Pt center. As this state corresponds to the HOMO at low dielectric constants, this is the cause of the strong solvatochromism calculated in this system. Interestingly, such a variation of the HOMO–LUMO gap is also obtained when we consider the [(tpphz)PtI$_2$] complex formed by the bridging ligand and the PtI$_2$ catalyst alone. Hence, the presence of the Ru^{II} center apparently is not the main cause for the occurrence of the strong solvatochromic effect.

Figure 3b shows the same properties as Figure 3a, but obtained with the FHI-AIMS code[31] for the RuPtI$_2$ complex in gas-phase and in acetonitrile (MeCN) using the so-called tight basis set. The results are very similar to those obtained with the Gaussian 16 code, in particular as far as the levels close to the HOMO–LUMO gap are concerned. This illustrates the robustness of our computational findings with respect to the strong solvatochromic effects found for the RuPtI$_2$ complex. Furthermore, as the tight basis set of FHI-AIMS yields triple zeta quality,[32] this favorable comparison strongly suggests that the Gaussian calculations with the chosen basis set yield reliable results.

In Figure 3c, finally the HOMO–LUMO gap is plotted as a function of the dielectric constant of the considered electrolytes. This panel illustrates that the HOMO–LUMO gap rises very strongly from 0.6 eV to 2.8 eV upon changing the dielectric constant from the gas-phase value of $\varepsilon \approx 1$ to $\varepsilon \approx 10$ corresponding to dichloroethane and then levels off at this value. This has to be related to the presence of the electric double

layer forming at the interface between the photocatalytic complex and the electrolyte.[33]

In order to get some more insights into the nature of the solvatochromic effect, we have determined local HOMO–LUMO gaps for three different pairs, Ru-bpy, Ru-tpphz, and Pt-tpphz, which are plotted in Figure 4a. Note that these local gaps are derived from the electronic structure of the whole complex by projecting it to the corresponding moieties of the complex. The local Ru-bpy HOMO–LUMO gap located around the photosensitizer is almost independent of the dielectric constant in spite of the fact that the levels are shifted as a function of the dielectric constant. This is caused by the fact that HOMO and LUMO are shifted by almost the same amount, as also found for ruthenium polypyridine complexes[21] and other organometallic compounds.[34]

In contrast, the local HOMO–LUMO gap decreases for the Ru-tpphz pair, whereas it increases for the Pt-tpphz pair for higher dielectric constants. A very similar increase is also observed for the Pt-tpphz pair of an isolated [(tpphz)PtI$_2$] complex, that is with the photosensitizer removed from the complex (Figure 4b). Hence, apparently this increase is independent of the coupling to the photosensitizer. According to Figure 4a, the minimum HOMO–LUMO gap changes at about $\varepsilon \approx 10$ from a Pt-tpphz to a Ru-tpphz transition, which means that in solvents with a low polarity the catalyst would possibly exhibit a higher photoactivity than the Ru complex. Furthermore, we analyzed the molecular orbital shapes, which are presented in detail in the Supporting Information, and hardly found any significant changes as a function of the dielectric constant of the solvent.

As solvatochromism is usually assumed to be due to the dipole-dipole interactions between polar molecules and a polarizable medium,[22] it is instructive to take a closer look at the dipole moment and the charge redistribution within the RuPtI$_2$ complex upon changing the dielectric constant of the solvent. As Figure 5a illustrates, there is a strong increase in the overall dipole moment of the whole complex from about 50D to 66D as a function of the polarity of the solvent. This increase strongly correlates with the opening up of the HOMO–LUMO gap shown in Figure 3c as a function of dielectric constant. This
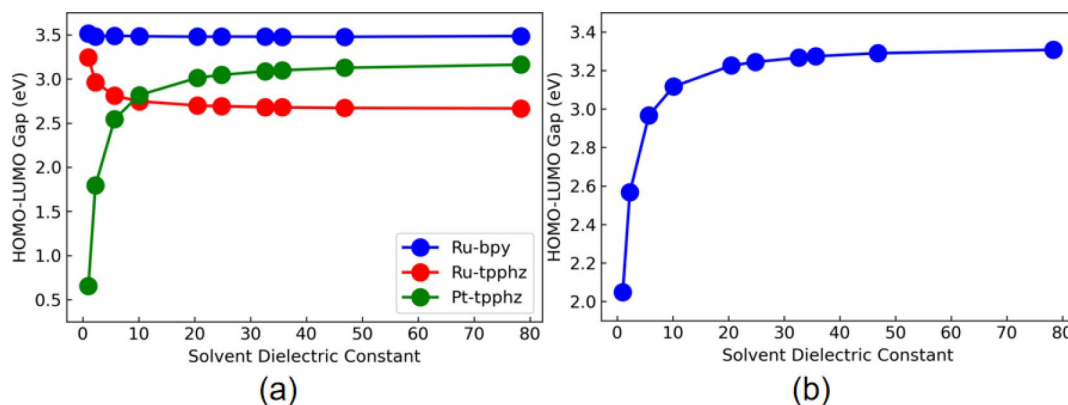

Figure 4. Local HOMO–LUMO gaps plotted as a function of the dielectric constant for (a) Ru-bpy, Ru-tpphz, and Pt-tpphz combinations and (b) for the Pt-tpphz pair of an isolated (tpphz)PtI$_2$ complex.
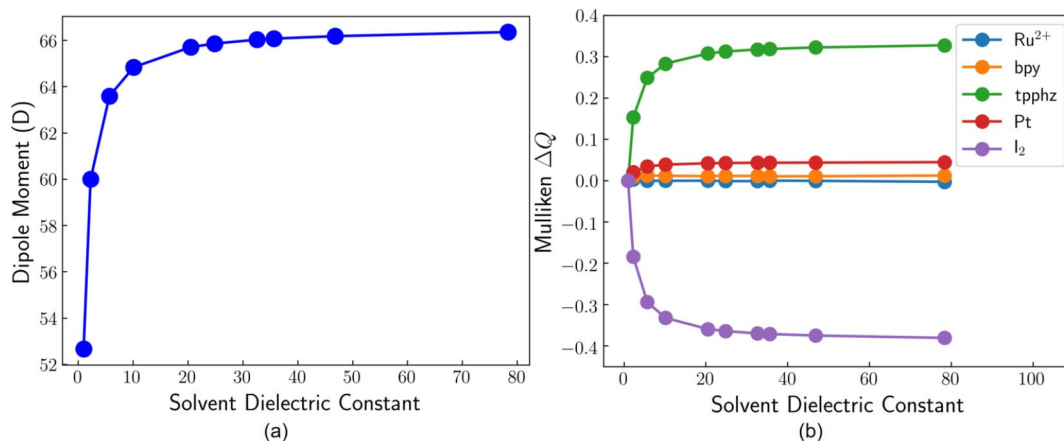
Chemistry–A European Journal

Research Article
doi.org/10.1002/chem.202302643

Chemistry
Europe
European Chemical
Societies Publishing

Figure 5. (a) Dipole moment and (b) Mulliken charge difference (ΔQ) of the RuPtI$_2$ complex as a function of dielectric constant of the solvent.

suggests that the change in the dipole moment is directly related to the strong solvatochromism of the whole complex.

In order to understand the cause of the increasing dipole moment, we have performed a Mulliken charge analysis focusing on five different parts of the photoactive complex, the Ru^{2+} ion, the bipyridine (bpy) moiety, the bridging ligand (tpphz), the Pt atom and the two iodine atoms. Note that Mulliken charges typically strongly depend on the choice of the basis set. However, any charge partition scheme is in principle ill-defined as their is no unique criterion to associate the electron distribution to one particular atom. However, the trends with respect to changes in the charges are rather robust and basically independent from the choice of the particular charge partition scheme. As Figure 5b reveals, upon variation of the dielectric constant the Mullikan charges at the Ru^{2+} ion, bipyridine (bpy), and the Pt atom remain approximately constant. In contrast, there is a significant charge transfer from the two iodine atoms to the bridging ligand upon increasing the dielectric constant. These findings suggest that the strong solvatochromism found in the RuPtI$_2$ complex is mainly due to the charge transfer from the iodine atoms to the bridging ligand upon increasing the dielectric constant of the solvent. This affects the energetics of the PtI$_2$-related states in a different way than all other states (Figure 3a) and thus causes the appearance of the strong solvatochromic effects.

Still, as Figure 3a reveals, the energy levels at the Ru^{2+} center, bipyridine, and tpphz strongly shift as a function of the dielectric constant. This might be an indication that the local charge at the Ru^{2+} and the ligands around Ru^{2+} are the cause for the overall shift of the energy levels whereas the local dipole moment between the bridging ligand and catalyst is responsible for the change of the HOMO–LUMO gap and thus the strong solvatochromism in this system. It is of course also interesting to consider how these observed solvatochromic effects affect the catalytic activity with respect to the hydrogen evolution reaction. However, as this would require a detailed study of the mechanistic details of this reaction, this issue is beyond the scope of this study. It is also fair to note that our understanding of these mechanistic details in the photocatalytic

water splitting is still rather limited and requires detailed independent studies.

In order to judge the quality of our calculations, we compare the absorption spectrum derived from the LR-TDDFT approach with the corresponding experimental results obtained in acetonitrile[3] in Figure 6. The main calculated absorption peaks in the visible range at 437 nm and in the UV range at 300 nm compare well with the corresponding experimental results, 442 nm and 280 nm, respectively, giving credibility to our approach. In Figure 6, we also identify the five main excitation mechanisms of the RuPtI$_2$ photocatalyst, namely the $d(Ru) \rightarrow \pi^*(tpphz)$ (blue), $d(Ru) \rightarrow \pi^*(bpy)$ (magenta), $d(Pt), n_I \rightarrow \pi^*(tpphz)$ (green), $\pi(tpphz) \rightarrow \pi^*(tpphz)$ (cyan), and $\pi(bpy) \rightarrow \pi^*(bpy)$ (orange) transitions. Electronic isosurfaces of the frontier orbitals of the RuPtI$_2$ photocatalyst in the considered solvents indicating the localization of the orbitals are shown in Figures S2–S11 in the Supporting Information. In the visible range, the peak at 437 nm represents the electronic excitation from Ru(II) to bipyridine, whereas the shoulder around 350–380 nm is related to the excitation from the catalyst to the bridging ligand. The UV peak at 300 nm is related to the superposition of intra-ligand charge transfer (ILCT) processes on the bridging ligand at 306 nm and in the bipyridine moiety at 277 nm.

The absorption spectra of the RuPtI$_2$ photocatalyst in various media within the UV-Vis range are shown in Figure 7a, the single excitations are listed in the Supporting Information in Tables S1–S10. Furthermore, we have collected the properties of the maximum excitations in the visible and the UV region in Table 1. Maximum absorption in the visible region occurs in the relatively narrow wavelength range between 428 and 438 nm (2.83–2.90 eV). The electronic excitation mechanisms are also basically the same, corresponding to $d(Ru) \rightarrow \pi^*(tpphz)$ and $d(Ru) \rightarrow \pi^*(bpy)$. Obviously, the solvent-solute interaction does not significantly influence the profile of the maximum excitation wavelengths of the RuPtI$_2$ photocatalysts within the visible region.

In detail, in the visible region, by increasing the dielectric constant corresponding to the transition from gas-phase to
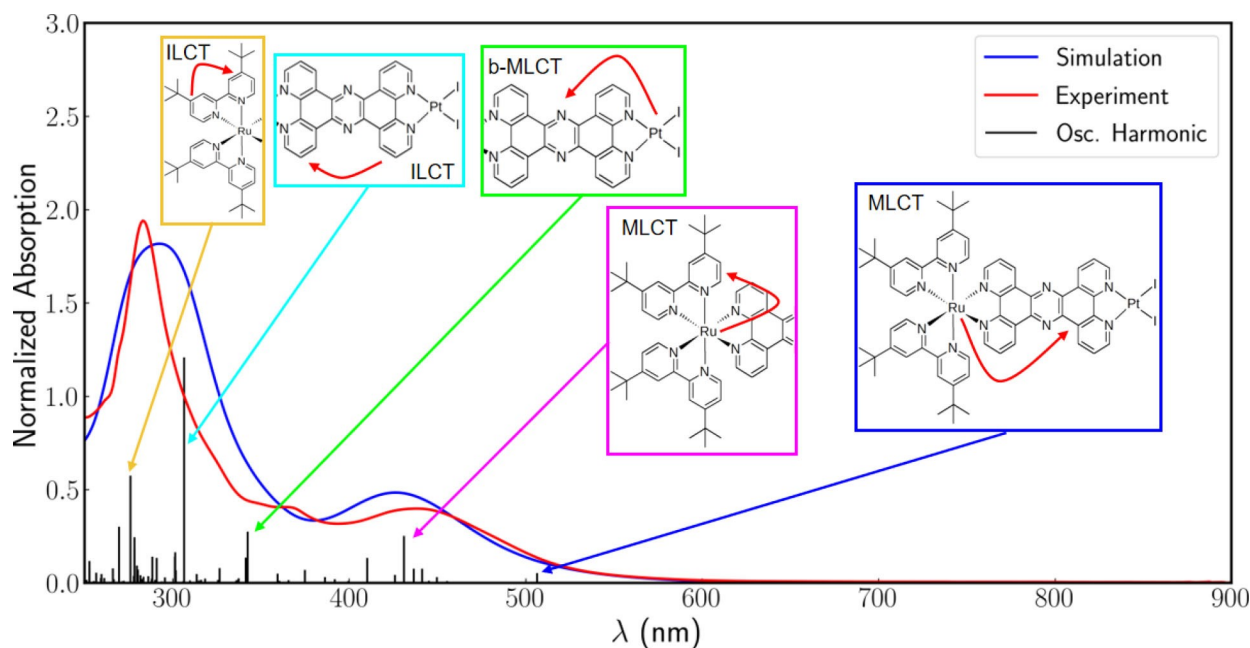
Figure 6. Experimental[3] and calculated absorption spectrum of RuPtI$_2$ in acetonitrile. The simulated spectrum plotted in blue is derived from the calculated single transitions shown as black bars by applying the typical resolution of the experiments. The insets illustrate the overall charge-transfer processes associated with five selected excitations derived from the calculations.
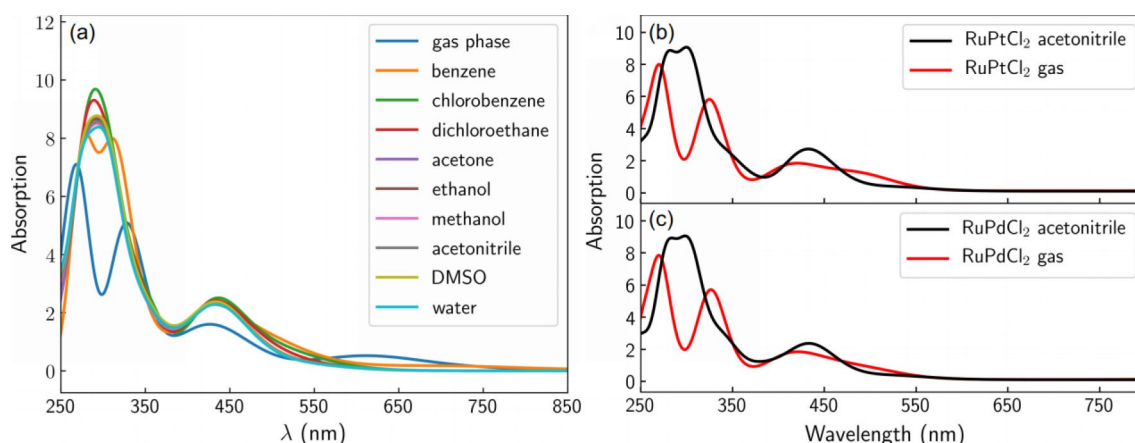

Figure 7. Calculated absorption spectra of (a) RuPtI$_2$ in various solvents, (b) RuPtCl$_2$ and (c) RuPdCl$_2$ in the gas-phase and acetonitrile.

chlorobenzene, there is an increase of the wavelength λ_{max}^{vis} of the main absorption peak which then stays approximately constant at about 435 nm for larger dielectric constants. As listed in detail in the Supporting Information, these excitations mainly correspond to d(Ru)$\rightarrow \pi^*$(tpphz) and d(Ru)$\rightarrow \pi^*$(bpy) transitions, except for chlorobenzene, where the largest contribution comes from the d(Pt)$\rightarrow \pi^*$(tpphz).

In order to examine the effect of the solvent on the singlet excitations of the photosensitizer, we define the maximum excitation energy of the photosensitizer (E_{max}^{PS}) as the transition with the maximum oscillator strength f_{PS} restricted to the transitions d(Ru)$\rightarrow \pi^*$(tpphz) and d(Ru)$\rightarrow \pi^*$(bpy) originating from the photosensitizer. According to Table 1, E_{max}^{PS} lies in the range 2.70–2.92 eV (453–424 nm). This means that the solvent variation does not significantly change the excitation energy of

the photosensitizer, as the maximum singlet absorption in the photosensitizer stays in the wavelength range of blue light for all considered dielectric constants. Interestingly enough, for low dielectric constants corresponding to gas-phase and benzene, in the UV region two ILCT peaks corresponding to the π(tpphz)$\rightarrow \pi^*$(tpphz) and π(bpy)$\rightarrow \pi^*$(bpy) transition are observed which merge to one peak at higher dielectric constants.

According to Figure 7a, in gas-phase and benzene the peaks at about 270 nm associated with the π-π^* excitation on the bipyridine moiety have a higher intensity than the corresponding excitation on tpphz at about 320 nm. As just mentioned, for higher dielectric constants of the solvent, only one peak appears in this region. This phenomenon is caused by the slight shift of the π-π^* transition on tetrapyrido phenazine from 3.9 eV to about 4.0 eV. On the other hand, the π(bpy)$\rightarrow \pi^*$(bpy)

Chemistry–A European Journal

Research Article
doi.org/10.1002/chem.202302643

Chemistry
Europe
European Chemical
Societies Publishing

Table 1. Properties of the main excitations of the solvated $RuPtI_2$ complexes in the considered solvents in the visible and UV region: wavelength in the visible (λ_{max}^{vis}) and in the UV region (λ_{max}^{UV}), excitation energy of the photosensitizer (E_{max}^{PS}) and from the catalyst to the bridging ligand (E_{max}^{ctbl}) together with their oscillator strengths f_{PS} and f_{ctbl}, respectively.

Solvent	ε	λ_{max}^{vis} (nm)	λ_{max}^{UV} (nm)	E_{max}^{PS} (eV)	f_{PS}	E_{max}^{ctbl} (eV)	f_{ctbl}
Gas-phase	1.00	427.00	328.00	2.73	0.16	2.01	0.14
			271.00				
Benzene	2.27	431.00	313.00	2.92	0.22	2.42	0.15
			278.00				
Chlorobenzene	5.70	436.00	289.00	2.91	0.13	2.85	0.20
Dichloroethane	10.12	434.00	285.00	2.87	0.18	3.02	0.12
Acetone	20.49	436.00	299.00	2.77	0.23	3.15	0.10
Ethanol	24.85	436.00	300.00	2.76	0.20	2.83	0.15
Methanol	32.61	436.00	300.00	2.76	0.18	3.20	0.14
Acetonitrile	35.69	435.00	300.00	2.77	0.18	3.21	0.13
DMSO	46.83	435.00	301.00	2.85	0.22	3.22	0.12
Water	78.36	435.00	301.00	2.85	0.20	3.25	0.12

transition tends to stay constant at ~4.4 eV. Thus these two ILCT states shift closer together resulting in only one overall peak. Furthermore, based on our TDDFT calculations we speculate that the small blue shift of the π(tpphz)$\rightarrow \pi^*$(tpphz) transition is probably related to the higher charge transfer to the bridging ligand for more polar solvents.

A rather similar qualitative behavior was observed in experiments in which gas-phase UV/Vis photofragmentation spectra where compared with normalized absorption spectra in acetonitrile solution, however, for $RuPdCl_2$ and $RuPtCl_2$ photocatalysts.[35] In order to check whether the results for $RuPdCl_2$ and $RuPtCl_2$ photocatalysts are also relevant for the understanding of the $RuPtI_2$ system we are focusing on here, we additionally performed LR-TDDFT calculations to determine the absorption spectra of the $RuPtCl_2$ and $RuPdCl_2$ complexes in gas-phase and acetonitrile (Figure 7b and 7c). Similar to the results for the $RuPtI_2$ system, we observe two peaks in the gas-phase and only one in acetonitrile for both photocatalysts. And again, the peaks in the UV region mainly originate from ILCTs in tetrapyrido phenazine and bipyridine. In addition, a MLCT peak is observed at ~440 nm, whereas a backward MLCT (b-MLCT) process from the catalyst to tetrapyrido phenazine (d(Pt), $n_I \rightarrow \pi^*$(tpphz)) leads to a shoulder at around 350 nm, in agreement with the experiment.[3,35,36] This nice agreement with the experiment for the $RuPdCl_2$ and $RuPtCl_2$ complexes suggests that our calculations for the $RuPtI_2$ complex are trustworthy, exhibiting a predictive power.

We now take a closer look at the backward MLCT (b-MLCT) from the catalyst to tetrapyrido phenazine (d(Pt), $n_I \rightarrow \pi^*$(tpphz)). As documented in the Supporting Information, a b-MLCT exists in solvents with small dielectric constants in the near-IR region up to the visible region, indicating a photo-poisoning effect. In solvents with high dielectric constants, on the other hand, b-MLCT occurs at wavelengths around 350 nm and shows up in measured spectra as a shoulder at this wavelength.[3] To quantify the behaviour of the b-MLCT, we define E_{max}^{ctbl} as the energy of the b-MLCT with maximum oscillator strength which are listed Table 1. We find that E_{max}^{ctbl} exhibits a blue-shift from 615 to 381 nm (2.01 to 3.25 eV) upon increasing the dielectric constant of the solvent from 1 to 80.

The b-MLCT from the catalyst metal center (Pt) to the bridging ligand is of importance as the efficiency of photocatalytic processes might also be influenced by such processes.[28] Electron transfer from the catalytic center to the bridging ligand can reduce the catalytic activity.[28] Hence, the b-MLCT transition should be energetically more demanding than the MLCT transition in order to suppress it. Indeed, as Table 1 shows, increasing the dielectric constant of the solvent to values above 10 shifts the excitation energy of the b-MLCT to the higher energy than those associated with the MLCT.

Besides addressing singlet transitions in the $RuPtI_2$ complex in various solvents, we have also considered singlet-triplet transitions which can play an important role in the excited state relaxation processes populating triplet MLCT states upon ultra-fast intersystem crossing.[27,28,37–39] The properties of the most dominant triplet excitations for the various solvents considered in this work are collected in the Supporting Information in Tables S6–S24. In general, we find trends in the excitations that are qualitatively rather similar to the singlet transitions, therefore we do no discuss them here in detail.

Overall, we find dramatic differences in the electronic properties of the $RuPtI_2$ complex embedded in an implicit solvent with low and high dielectric constants. The HOMO–LUMO gap, the dipole moment, and the charge of the $RuPtI_2$ complex in the singlet state change rather significantly at low dielectric constants upon increasing the dielectric constant (Figures 3–5). In total, all these changes appear to be a consequence of the charge rearrangement between the tpphz bridging ligand and the two iodine atoms of the catalytically active center upon embedding the $RuPtI_2$ complex in a polarizable medium (Figure 5b). As these solvatochromic effects can be used to tailor the electronic properties of photoactive complexes, it appears to be worthwhile to also look for such a

Chemistry–A European Journal

Research Article
doi.org/10.1002/chem.202302643

Chemistry
Europe
European Chemical
Societies Publishing

solvatochromism in other photoactive and photocatalytic complexes.

Conclusions

Based on density functional theory (DFT) and time-dependent DFT calculations, we have studied the properties of a RuPtI$_2$ molecular photocatalyst upon embedding it in an implicit solvent as a function of its dielectric constant. Whereas the geometric structure of the RuPtI$_2$ complex is hardly influenced by this embedding, the electronic properties change dramatically upon increasing the dielectric constant from 1 to 20, corresponding to the transition from gas-phase conditions to solvation in acetone. For higher dielectric constants, the properties then remain approximately constant. These dramatic changes at low dielectric constants are associated with a change in the location of the HOMO state from the PtI$_2$ catalyst to the photoactive Ru center and a strong increase in the HOMO–LUMO gap. Based on an analysis of the charge and spin distribution, we relate these changes to the net electron transfer from the bridging ligand to the iodine atoms upon embedding the RuPtI$_2$ complex in a polarizable medium. As a consequence, we predict strong solvatochromism in this complex. Such dramatic effects might well also occur in other photoactive and photocatalytic complexes upon solvation. As the integration of photocatalysts in very nonpolar polymeric materials, lipid membranes, etc. is an area of increasing relevance, integration of RuPtI$_2$ and similar photocatalysts in such materials has to be treated with caution, as a complete switch of the light-induced electron transfer mechanisms might occur. However, in general our results suggest that such strong solvatochromic effects might be used to deliberately tailor the properties of photoactive complexes.

Computational Details

In order to unravel the effect of the interaction between molecular RuPtI$_2$ photocatalysts and its surrounding medium, we have performed DFT and TDDFT calculations using the Gaussian 16 code[29] in a setup that corresponds to the present standard in the field of computational molecular photocatalysis.[11,40–42] The electronic ground-state properties of the RuPtI$_2$ complexes in the singlet and triplet configurations were determined using DFT calculations employing the B3LYP functional[43,44] to account for the exchange-correlation effects using the def2svp basis set[45,46] for all atoms. To take dispersion interaction into account, the D3 dispersion scheme of Grimme with Becke–Johnson damping was used in this work.[47,48] Note that this computational methodology used in our work is widely employed in this field, see, e.g., Refs. [11,40–42], and yields results that compare favorably with measured data. Some additional calculations have also been performed with the FHI-AIMS code.[31] In the AIMS calculations, the tight basis set was employed for the B3LYP geometry optimization and energy level calculations. Relativistic effects have been considered on the level of the atomic zeroth order regular approximation (ZORA).[49] Upon including relativistic effects, the energies of the considered singlet and triplet states changed by less than 25 meV, and no change in the ordering of the transitions

was observed. Furthermore, the van der Waals correction scheme by Tkatchenko and Scheffler (vdW-TS) was used.[50] To model the presence of the electrolyte in the AIMS calculation, we used the multipole moment expansion (MPE) implicit solvation method.[51] Using test sets from Marenich et al.,[52] we selected the solvation parameters $\alpha = 2.89$ meV/Å^2, $\beta = -3.12$ meV/Å^3 and the cavity isodensity $\rho_{iso} = 40.00$ meV/Å$^{3[53]}$ for acetonitrile. Further details of this procedure are given in the Supporting Information.

In the Gaussian calculations, the SMD (Solvation Model Based on Density) continuum solvation model[52] was applied to describe the solvent around the complex as it gives more reliable values of the solvation free energies (ΔG_{sol}) of cationic complexes compared to other methods such as the integral-equation-formalism polarizable continuum model (IEFPCM) or conductor-like polarizable continuum models (CPCM).[52] Furthermore, it also promises a more realistic representation of the molecule-solvent interaction as also other properties such as Abraham's hydrogen bond acidity and basicity, aromaticity, and electronegative halogenicity have entered its construction.[29,52] The particular solvents addressed in this work are characterized by their respective dielectric constant. In detail, we considered benzene ($\varepsilon = 2.27$), chlorobenzene ($\varepsilon = 5.70$), DCE ($\varepsilon = 10.12$), acetone ($\varepsilon = 20.49$), EtOH ($\varepsilon = 24.85$), MeOH ($\varepsilon = 32.61$), MeCN ($\varepsilon = 35.69$), DMSO ($\varepsilon = 46.83$) and water ($\varepsilon = 78.36$). Furthermore, the corresponding results are also compared with gas-phase calculations (gas, $\varepsilon = 1.00$) calculations. In principle it would be desirable to validate the results of the implicit solvent calculations with simulations considering explicit solvent molecules. However, this would require sampling over ab initio molecular dynamics simulations with sufficiently long run times including several hundreds of explicit solvent molecules. This is at the moment still numerically prohibitive with existing computer resources.

The optical properties of the RuPtI$_2$ complexes were derived using a linear response formalism based on time-dependent density functional theory (LR-TDDFT)[54,55] within the singlet ground-state geometry of the complexes. The absorption spectra of the RuPtI$_2$ complexes were determined using:

$$\varepsilon(E) = \sum_{i}^{n} \frac{f}{\sigma} \exp\left(-\frac{E - E_i}{\sigma}\right)^2, \tag{3}$$

where $\varepsilon(E)$ corresponds to the absorption spectra at energy E, f is the oscillator harmonic strength derived in the TDDFT calculations, and σ denotes the broadening of the absorption spectra.[29] In this work, we selected $\sigma = 0.30$ eV in Equation (3) in order to mimic the typical resolution of experiments.

To further validate our computational approach, we used the RuPtI$_2$ geometry optimized with the B3LYP[43,44] functional and performed for this geometry single-point calculations for the HOMO–LUMO gap in the gas-phase and in acetonitrile using further hybrid functionals (PB0,[56] HSE06[57] and M06[58]), a long-range-corrected (CAM-B3LYP[59]) and a double hybrid functionals (M06-2X[60]). Interestingly, B3LYP, PBE0 and M06 yield rather similar results for the two energy gaps, whereas HSE06 gives a smaller gap (Figure S16). In contrast, the long-range-corrected (CAM-B3LYP) and the double hybrid (M06-2X) functionals both predict gaps that are about twice as large as the B3LYP results.

In order to allow a better comparison with experiment, we determined the optical properties of the RuPtI$_2$ complex for the different functional using TDDFT calculations, again using the relaxed B3LYP geometry. The optical spectra shown in Figure S17 demonstrate that the hybrid functionals B3LYP, PBE0 and M06 nicely reproduce the experimental spectrum, in particular also the experimental MLCT absorbance in the visible regime at $\lambda_{max} =$

Chemistry–A European Journal

Research Article
doi.org/10.1002/chem.202302643

Chemistry Europe
European Chemical
Societies Publishing

442 nm, whereas the HSE, CAM-B3LYP, and M06-2X functionals all yield overall blue-shifted spectra. Given the agreement with the experimental absorption spectra, we conclude that the B3LYP functional chosen by us as well as the PBE0 and M06 functionals are well-suited to describe the electronic properties and excitations RuPtI$_2$ complex.

Supporting Information

The authors have cited additional references within the Supporting Information.[61–64]

Acknowledgements

Conflict of Interests

The authors declare no conflict of interest.

Data Availability Statement

The data that support the findings of this study are available from the corresponding author upon reasonable request.

Keywords: highest occupied molecular orbital · implicit solvent · photocatalysis · quantumchemistry · solvatochromism

[1] R. Schlögl, *ChemSusChem* **2010**, *3*, 209–222.
[2] V. Balzani, A. Juris, M. Venturi, S. Campagna, S. Serroni, *Chem. Rev.* **1996**, *96*, 759–834.
[3] M. G. Pfeffer, T. Kowacs, M. Wächtler, J. Guthmuller, B. Dietzek, J. G. Vos, S. Rau, *Angew. Chem. Int. Ed.* **2015**, *54*, 6627–6631.
[4] S. Kaufhold, L. Petermann, R. Staehle, S. Rau, *Coord. Chem. Rev.* **2015**, *304–305*, 73–87.
[5] K. E. Dalle, J. Warnan, J. J. Leung, B. Reuillard, I. S. Karmel, E. Reisner, *Chem. Rev.* **2019**, *119*, 2752–2875.
[6] A. Sen, S. Kupfer, S. Gräfe, A. Groß, *J. Phys. B: At. Mol. Opt. Phys.* **2020**, *53*, 234001.
[7] R. A. Wahyuono, B. Seidler, S. Bold, A. Dellith, J. Dellith, J. Ahner, P. Wintergerst, G. Lowe, M. D. Hager, M. Wächtler, C. Streb, U. S. Schubert, S. Rau, B. Dietzek, *Sci. Rep.* **2021**, *11*, 2787.
[8] M. H. Putra, S. Seidenath, S. Kupfer, S. Gräfe, A. Groß, *Chem. Eur. J.* **2021**, *27*, 17104–17114.
[9] A. Sen, M. H. Putra, A. K. Biswas, A. K. Behera, A. Groß, *Dyes Pigm.* **2023**, *213*, 111087.
[10] A. Sen, A. Groß, *Int. J. Quantum Chem.* **2019**, *119*, e25963.
[11] M. G. Pfeffer, C. Müller, E. T. E. Kastl, A. K. Mengele, B. Bagemihl, S. S. Fauth, J. Habermehl, L. Petermann, M. Wächtler, M. Schulz, D. Chartrand, F. Laverdière, P. Seeber, S. Kupfer, S. Gräfe, G. S. Hanan, J. G. Vos, B. Dietzek-Ivanšić, S. Rau, *Nat. Chem.* **2022**, *14*, 500–506.
[12] J. Habermehl, D. Naaroozi, M. Martynow, Y. E. Vilk, R. Beranek, J. Guthmuller, S. Rau, *Sustain. Energy Fuels* **2020**, *4*, 619–624.
[13] M. G. Pfeffer, C. Pehlken, R. Staehle, D. Sorsche, C. Streb, S. Rau, *Dalton Trans.* **2014**, *43*, 13307–13315.
[14] A. K. Mengele, D. Weixler, A. Chettri, M. Maurer, F. L. Huber, G. M. Seibold, B. Dietzek, B. J. Eikmanns, S. Rau, *Chem. Eur. J.* **2021**, *27*, 16840–16845.
[15] C. Pehlken, M. G. Pfeffer, K. Reich, S. Rau, *Photochem. Photobiol.* **2022**, *98*, 1255–1263.
[16] S. Rau, B. Schäfer, D. Gleich, E. Anders, M. Rudolph, M. Friedrich, H. Görls, W. Henry, J. G. Vos, *Angew. Chem. Int. Ed.* **2006**, *45*, 6215–6218.
[17] C. Herrmann, J. Neugebauer, M. Presselt, U. Uhlemann, M. Schmitt, S. Rau, J. Popp, M. Reiher, *J. Phys. Chem. B* **2007**, *111*, 6078–6087.
[18] S. Tschierlei, M. Karnahl, M. Presselt, B. Dietzek, J. Guthmuller, L. González, M. Schmitt, S. Rau, J. Popp, *Angew. Chem. Int. Ed.* **2010**, *49*, 3981–3984.
[19] M. K. Nazeeruddin, S. M. Zakeeruddin, R. Humphry-Baker, M. Jirousek, P. Liska, N. Vlachopoulos, V. Shklover, C.-H. Fischer, M. Grätzel, *Inorg. Chem.* **1999**, *38*, 6298–6305.
[20] S. Fantacci, F. De Angelis, A. Selloni, *J. Am. Chem. Soc.* **2003**, *125*, 4381–4387.
[21] M.-F. Charlot, A. Aukauloo, *J. Phys. Chem. A* **2007**, *111*, 11661–11672.
[22] C. Reichardt, *Chem. Rev.* **1994**, *94*, 2319–2358.
[23] A. Marini, A. Muñoz Losa, A. Biancardi, B. Mennucci, *J. Phys. Chem. B* **2010**, *114*, 17128–17135.
[24] A. Masternak, G. Wenska, J. Milecki, B. Skalski, S. Franzen, *J. Phys. Chem. A* **2005**, *109*, 759–766.
[25] T. Liu, W.-G. Han, F. Himo, G. M. Ullmann, D. Bashford, A. Toutchkine, K. M. Hahn, L. Noodleman, *J. Phys. Chem. A* **2004**, *108*, 3545–3555.
[26] P. Krawczyk, *J. Mol. Model.* **2015**, *21*, 118.
[27] M. Martynow, S. Kupfer, S. Rau, J. Guthmuller, *Phys. Chem. Chem. Phys.* **2019**, *21*, 9052–9060.
[28] L. Zedler, A. K. Mengele, K. M. Ziems, Y. Zhang, M. Wächtler, S. Gräfe, T. Pascher, S. Rau, S. Kupfer, B. Dietzek, *Angew. Chem. Int. Ed.* **2019**, *58*, 13140–13148.
[29] M. J. Frisch, G. W. Trucks, H. B. Schlegel, G. E. Scuseria, M. A. Robb, J. R. Cheeseman, G. Scalmani, V. Barone, G. A. Petersson, H. Nakatsuji, X. Li, M. Caricato, A. V. Marenich, J. Bloino, B. G. Janesko, R. Gomperts, B. Mennucci, H. P. Hratchian, J. V. Ortiz, A. F. Izmaylov, J. L. Sonnenberg, D. Williams-Young, F. Ding, F. Lipparini, F. Egidi, J. Goings, B. Peng, A. Petrone, T. Henderson, D. Ranasinghe, V. G. Zakrzewski, J. Gao, N. Rega, G. Zheng, W. Liang, M. Hada, M. Ehara, K. Toyota, R. Fukuda, J. Hasegawa, M. Ishida, T. Nakajima, Y. Honda, O. Kitao, H. Nakai, T. Vreven, K. Throssell, J. A. Montgomery Jr, J. E. Peralta, F. Ogliaro, M. J. Bearpark, J. J. Heyd, E. N. Brothers, K. N. Kudin, V. N. Staroverov, T. A. Keith, R. Kobayashi, J. Normand, K. Raghavachari, A. P. Rendell, J. C. Burant, S. S. Iyengar, J. Tomasi, M. Cossi, J. M. Millam, M. Klene, C. Adamo, R. Cammi, J. W. Ochterski, R. L. Martin, K. Morokuma, O. Farkas, J. B. Foresman, D. J. Fox, Gaussian 16 Revision C.01, **2016**, Gaussian Inc. Wallingford CT.
[30] M. K. Brennaman, J. H. Alstrum-Acevedo, C. N. Fleming, P. Jang, T. J. Meyer, J. M. Papanikolas, *J. Am. Chem. Soc.* **2002**, *124*, 15094–15098.
[31] V. Blum, R. Gehrke, F. Hanke, P. Havu, V. Havu, X. Ren, K. Reuter, M. Scheffler, *Comp. Phys. Commun.* **2009**, *180*, 2175–2196.
[32] S. R. Jensen, S. Saha, J. A. Flores-Livas, W. Huhn, V. Blum, S. Goedecker, L. Frediani, *J. Phys. Chem. Lett.* **2017**, *8*, 1449–1457.
[33] A. Groß, S. Sakong, *Curr. Opin. Electrochem.* **2019**, *14*, 1–6.
[34] S. A. Miresmaeili, R. Ghiasi, *Russ. J. Phys. Chem.* **2017**, *91*, 1026–1036.
[35] D. Imanbaew, J. Lang, M. F. Gelin, S. Kaufhold, M. G. Pfeffer, S. Rau, C. Riehn, *Angew. Chem. Int. Ed.* **2017**, *56*, 5471–5474.
[36] M. G. Pfeffer, B. Schäfer, G. Smolentsev, J. Uhlig, E. Nazarenko, J. Guthmuller, C. Kuhnt, M. Wächtler, B. Dietzek, V. Sundström, S. Rau, *Angew. Chem. Int. Ed.* **2015**, *54*, 5044–5048.
[37] A. K. Mengele, C. Müller, D. Naaroozi, S. Kupfer, B. Dietzek, S. Rau, *Inorg. Chem.* **2020**, *59*, 12097–12110.
[38] E. Giannoudis, S. Bold, C. Müller, A. Schwab, J. Bruhnke, N. Queyriaux, C. Gablin, D. Leonard, C. Saint-Pierre, D. Gasparutto, D. Aldakov, S. Kupfer, V. Artero, B. Dietzek, M. Chavarot-Kerlidou, *ACS Appl. Mater. Interfaces* **2021**, *13*, 49802–49815.
[39] S. S. Nair, O. A. Bysewski, S. Kupfer, M. Wächtler, A. Winter, U. S. Schubert, B. Dietzek, *Inorg. Chem.* **2021**, *60*, 9157–9173.

[40] G. E. Shillito, S. Rau, S. Kupfer, *ChemCatChem* **2023**, *15*, e202201489.

[41] Y. Liu, A. Feng, R. Zhu, D. Zhang, *Chem. Sci.* **2023**, *14*, 4580–4588.

[42] B. Chandra Garain, S. K. Pati, *ChemPhysChem* **2023**, *24*, e202200753.

[43] C. Lee, W. Yang, R. G. Parr, *Phys. Rev. B* **1988**, *37*, 785–789.

[44] A. D. Becke, *J. Chem. Phys.* **1993**, *98*, 5648–5652.

[45] F. Weigend, R. Ahlrichs, *Phys. Chem. Chem. Phys.* **2005**, *7*, 3297–3305.

[46] F. Weigend, *Phys. Chem. Chem. Phys.* **2006**, *8*, 1057–1065.

[47] S. Grimme, S. Ehrlich, L. Goerigk, *J. Comb. Chem.* **2011**, *32*, 1456–1465.

[48] D. Mahlberg, S. Sakong, K. Forster-Tonigold, A. Groß, *J. Chem. Theory Comput.* **2019**, *15*, 3250–3259.

[49] E. van Lenthe, E. J. Baerends, J. G. Snijders, *J. Chem. Phys.* **1994**, *101*, 9783–9792.

[50] A. Tkatchenko, M. Scheffler, *Phys. Rev. Lett.* **2009**, *102*, 073005.

[51] M. Sinstein, C. Scheurer, S. Matera, V. Blum, K. Reuter, H. Oberhofer, *J. Chem. Theory Comput.* **2017**, *13*, 5582–5603.

[52] A. V. Marenich, C. J. Cramer, D. G. Truhlar, *J. Phys. Chem. B* **2009**, *113*, 6378–6396.

[53] C. Hille, S. Ringe, M. Deimel, C. Kunkel, W. E. Acree, K. Reuter, H. Oberhofer, *J. Chem. Phys.* **2019**, *150*, 041710.

[54] C. Adamo, D. Jacquemin, *Chem. Soc. Rev.* **2013**, *42*, 845–856.

[55] A. D. Laurent, C. Adamo, D. Jacquemin, *Phys. Chem. Chem. Phys.* **2014**, *16*, 14334–14356.

[56] C. Adamo, V. Barone, *J. Chem. Phys.* **1999**, *110*, 6158–6170.

[57] J. Heyd, G. E. Scuseria, M. Ernzerhof, *J. Chem. Phys.* **2006**, *124*, 219906.

[58] Y. Zhao, D. G. Truhlar, *Theor. Chem. Acc.* **2007**, *120*, 215–241.

[59] T. Yanai, D. P. Tew, N. C. Handy, *Chem. Phys. Lett.* **2004**, *393*, 51–57.

[60] Y. Zhao, D. G. Truhlar, *Theor. Chem. Acc.* **2008**, *119*, 525–525.

[61] J.-L. Fattebert, F. Gygi, *J. Comput. Chem.* **2002**, *23*, 662–666.

[62] O. Andreussi, I. Dabo, N. Marzari, *J. Chem. Phys.* **2012**, *136*, 064102.

[63] J. G. Kirkwood, *J. Chem. Phys.* **1934**, *2*, 351–361.

[64] C. Hille, S. Ringe, M. Deimel, C. Kunkel, W. E. Acree, K. Reuter, H. Oberhofer, *J. Chem. Phys.* **2019**, *150*, 041710.

RESEARCH ARTICLE

Solvatochromism denotes the dependence of the colour of a solution on the solvent. Based on quantum chemical calculations, we predict strong solvatochromism in a light-driven molecular photocatalyst for hydrogen evolution. Moreover, we find a solvent-dependent relocation of the highest occupied molecular orbital opening the way to deliberately modify the properties of photo-active complexes.
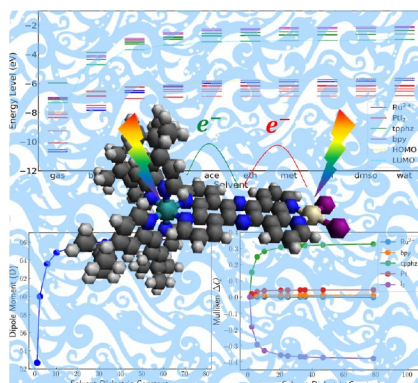
M. H. Putra, B. Bagemihl, Prof. Dr. S. Rau, Prof. Dr. A. Groß*

1 – 11

Prediction of Strong Solvatochromism in a Molecular Photocatalyst